Journal of Thermal Biology 81 (2019) 178–184

Contents lists available at ScienceDirect

Journal of Thermal Biology

journal homepage: www.elsevier.com/locate/jtherbio

Measurement of human body surface heat flux using a calorimetric sensor

Pedro Jesús Rodríguez de Rivera, Miriam Rodríguez de Rivera, Fabiola Socorro, Manuel Rodríguez de Rivera*

Departamento de Física, Universidad de Las Palmas de Gran Canaria, E-35017 Las Palmas, de Gran Canaria, Spain

ARTICLE INFO

Keywords:
Direct calorimetry
Heat conduction calorimeters
Isothermal calorimeters, Medical calorimetry
Non-differential calorimeters
Physiology

ABSTRACT

We have developed a calorimetric sensor that can perform local measurements of the heat flux transmitted by conduction between a human body and thermostat located inside the sensor. The sensor has a detection area of $2 \times 2\,cm^2$ and, in its current configuration, facilitates measurement with a resolution of 10 mW. In this paper, measurements of two healthy male subjects of different ages (24 and 60 years) are presented. We study the variation in the power dissipated by the human body surface as a function of time for a thermostat temperature of 28 °C. We also study the same power with thermostat temperatures varying from 24° to 36°C. Measurements are performed on three different surface areas of the human body: the sternum, abdomen, and hand. The ambient room temperature during all measurements was in the range of 22–24 °C, and the subjects were seated and resting. The results show that the heat flux in the trunk is much more stable than that in the hand and that the heat flux in the sternum is greater than that in other areas. Additionally, this flux is higher in the younger subject ($42\,mW/cm^2$) than in the older subject ($35\,mW/cm^2$). We also defined a thermal parameter that represents the thermal resistance between the sensor thermostat and the skin. The mean value of this parameter varies between 51 and 71 K/W depending on the subject and measurement area.

1. Introduction

It is of significant interest to investigate the magnitudes of thermal energy and heat flow produced in physical, chemical, or biological processes. The measurement of such magnitudes is typically performed using calorimetric instruments that attempt to reproduce a process by isolating it from undesirable perturbations. However, reproducing a process in a single instrument is not always easy. Therefore, specific instruments are designed for different processes. A wide variety of instruments have been constructed for various applications and sets of applications. (Wendlandt, 1974; Handbook of Thermal Analysis and Calorimetry: Principles and Practice, 1998). The calorimetric sensor we developed (Socorro et al., 2017) measures the heat flow from a defined skin area on the human body. In this case, the thermal process does not take place inside the calorimeter. Instead, the calorimeter is placed on the skin to measure heat flux. This is a direct measurement of the human body response (in terms of heat power) to the stimulation of placing the device on the skin. Based on the principles of Hansen classification (Hansen, 2001), we can include this sensor in the group of non-differential isothermal heat-conduction calorimeters.

Based on the emergence of digital infrared cameras, a considerable amount of research has been devoted to the measurement of body surface temperature (Lahiri et al., 2012). In some cases, this research is conducted to study the interaction between human thermophysiology and an external environment (Livingston et al., 1987). In other cases, local temperatures can be used to monitor and detect inflammation associated with knee replacement (Haidar et al., 2006; Mehra et al., 2005), rheumatoid arthritis (Rajapakse et al., 1981), osteoarthritis (Denoble et al., 2010), allergies (Rokita et al., 2011), frozen shoulders (Vecchio et al., 1992), and tendinitis (Miyakoshi et al., 1998). Additionally, this technology has been applied to the diagnosis of skin cancer by using longwave infrared cameras (Godoy et al., 2017). Therefore, measurements captured by a calorimetry mini sensor can serve as a valuable complement to pathological studies.

The calorimetric sensor used in this study has been described in two previous papers. The first (Socorro et al., 2016) described its elements and operating principles and the second (Socorro et al., 2017) described a method for determining the heat flux passing across the sensor as a function of time, beginning from the instant the sensor is placed on the measurement surface. In this paper, measurements of two healthy male subjects of different ages (24 and 60 years) are presented. We study the variation in the power dissipated by the human body as a function of

* Corresponding author.
E-mail addresses: pedrojrdrs@gmail.com (P.J.R. de Rivera), miriam.mrdrs@gmail.com (M.R. de Rivera), fabiola.socorro@ulpgc.com (F. Socorro), manuel.rguezderivera@ulpgc.com (M.R. de Rivera).

https://doi.org/10.1016/j.jtherbio.2019.02.022
Received 9 October 2018; Received in revised form 24 February 2019; Accepted 27 February 2019
Available online 28 February 2019

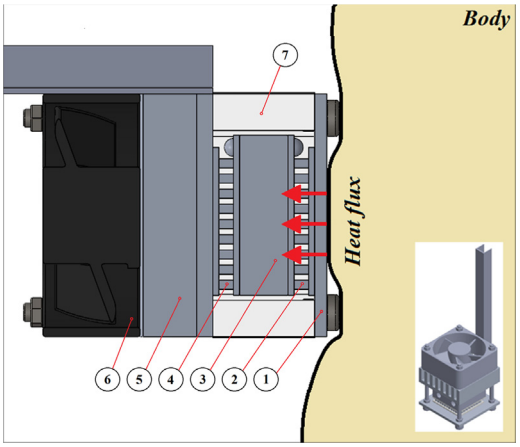

Fig. 1. Schematic of the calorimetric sensor: 1) aluminium plate, 2) measurement thermopile based on the Seebeck effect, 3) thermostat containing an RTD sensor and heat resistor, 4) cooling thermopile based on the Peltier effect, 5) aluminium heat sink, 6) fan, and 7) thermal insulation.

time for a thermostat temperature of 28 °C. We also study the same power with thermostat temperatures varying from 24° to 36°C. Measurements were performed on three parts of the human body: the sternum, abdomen, and hand. The ambient room temperature was in the range of 22–24 °C and the subjects were seated and resting.

This paper is organised as follows. First, we describe the sensor and measurement procedure. Next, we discuss the method used for determination of the heat power detected by the sensor. Finally, we present experimental results.

2. Calorimetric sensor

The purpose of the calorimetric sensor is to measure the heat flux transmitted by conduction between the human body and a thermostat located inside the sensor. The measurement surface has an area of $2 \times 2\,cm^2$. Fig. 1 presents a schematic of the sensor. The red arrows indicate that the heat flux measured by the sensor is only that which pass across the sensor. The core of the sensor consists of a measurement thermopile (part two in Fig. 1) placed between a measuring plate (part one in Fig. 1) and thermostat (part three in Fig. 1). This thermostat consists of a small aluminium block that contains a resistance temperature detector (RTD) sensor (Pt-100) and a constantan heat resistor. To perform temperature control, there is a cooling system attached to the thermostat. The cooling system consists of another thermopile (part four in Fig. 1) and a heat sink with a fan (parts five and six, respectively, in Fig. 1). The measurement thermopile, thermostat, and cooling thermopile are thermally insulated from the outside (part seven in Fig. 1). The thermostat temperature is kept constant by a proportional-integral-derivative (PID) controller (Ogata, 2010), which can maintain the programmed temperature with a resolution of ± 5 mK. The sensor elements, measurement and control instrumentation, operating domain, and sensor resolution are described in detail in previous papers (Socorro et al., 2016, 2017).

Based on the Seebeck effect, the measurement thermopile generates a calorimetric signal $y\ (t)$ in millivolts. This signal is related to the power dissipated in the thermostat to maintain a constant temperature (W_{pid}) and the heat power generated by the human body that passes across the sensor (W_{body}). The first power (W_{pid}) is known because it is calculated by the PID temperature controller and the second power (W_{body}) is the value we wish to measure. Therefore, we can consider the device as a system with two inputs (the powers W_{pid} and W_{body}) and one output (calorimetric signal). Having experimentally proven the linearity of the system (Socorro and de Rivera, 2010; Jesús et al., 2013a, 2013b), we can relate the calorimetric output to the input powers as

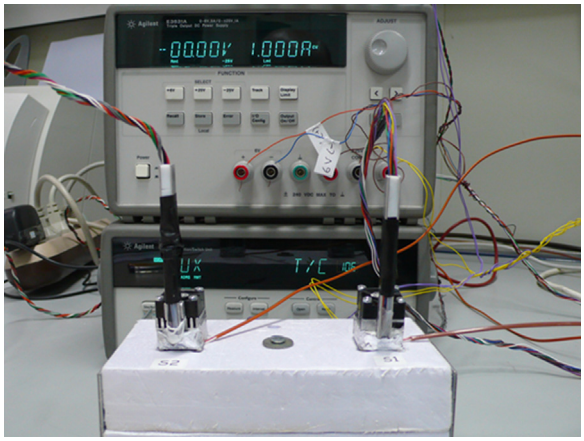

Fig. 2. Calorimetric sensors on their bases, and measurement and control instrumentation.

follows

$$a_2\frac{d^2y(t)}{dt^2} + a_1\frac{dy(t)}{dt} + y(t) = K_1\left(b_1\frac{dW_{body}(t)}{dt} + W_{body}(t)\right) + K_2\left(b_2\frac{dW_{pid}(t)}{dt} + W_{pid}(t)\right), \quad (1)$$

Sensor calibration consists of the determination of the coefficients in Eq. (1). The sensitivities K_1 and K_2 define the steady-state response of the sensor and the coefficients a_i and b_i define the transient response. We have a calibration base constructed from a thermal insulating material that was specially designed for this calibration procedure. Additionally, this base includes a magnetic holder for easy use and a Joule resistor for calibration. Fig. 2 presents a photograph of the two sensors on the calibration base, as well as the measurement and control instrumentation. The method and results of calibration were described in previous papers (Socorro et al., 2016, 2017). Table 1 lists the values of the coefficients for Eq. (1) for each sensor. Sensor resolution is determined based on the signal noise in the steady state using the equation $K_1\Delta W_{body} + K_2\Delta W_{pid} = \Delta y$. From $\Delta y = \pm\ 0.10$ mV and $\Delta W_{pid} = \pm\ 10$ mW, we obtain a sensor resolution of $\Delta W_{body} \approx 6.0$ mW for these values. Considering the uncertainty in the calculated sensitivities during different calibrations, we have a final resolution lower than 10 mW.

3. Heat flux determination and measurement procedure

Several methods can be used to determine the heat flux $W_{body}\ (t)$ by using Eq. (1), the power dissipated in the thermostat $W_{pid}\ (t)$, and a known calorimetric signal $y\ (t)$. The first method consists of replacing the known curves in the equation to obtain $W_{body}\ (t)$, but in this case, the derivatives of the calorimetric signal and power W_{pid} excessively amplify the existing noise in the signals. For this reason, we chose a method consisting of the reconstruction of the calorimetric signal from the input powers using Eq. (1). This requires iterative minimisation of the squared error between the experimental and calculated calorimetric

Table 1
Results of the calibration of sensors S1 and S2 (parameters for Eq. (1)).

Parameter	S1	S2	units
K_1	110.5	124.9	$mV\,W^{-1}$
K_2	− 54.2	− 44.2	$mV\,W^{-1}$
a_1	96.8	98.4	s
a_2	906.2	1029.4	s^2
b_1	67.3	76.1	s
b_2	111.0	100.0	s

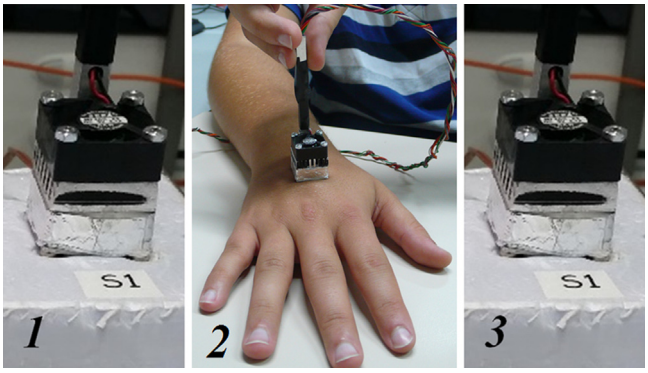

Fig. 3. Measurement procedure: 1) sensor on its base, 2) sensor on the body, 3) sensor on its base.

signals. This was achieved using the Nelder–Mead simplex search algorithm (Nelder and Mead, 1965) and MatLab software (Optimization ToolboxTM User's Guide, 2004). To find the parameters of W_{body} (t) that minimise the error criterion, this method requires knowledge regarding the functional expression of W_{body} (t). We propose a mathematical model (Socorro et al., 2017) that represents the heat flux of the human body surface that passes across the sensor, which is defined by the sum of a series of exponentials as $W_{body}\ (t) = A_0 + \Sigma\ A_i\ exp\ (-t/\tau_i)$.

This calculation procedure requires an initial steady state that ensures the knowledge of the signals and their derivatives at the initial moment. Therefore, we propose a measurement procedure with three phases (Jesús et al., 2013a, 2013b). First, the sensor is placed on the calibration base until a steady state is reached for the set thermostat temperature. Second, the sensor is placed on the body surface where the measurement is intended to be performed. Third, the sensor is again placed on its calibration base until it returns to a steady state. Each phase lasts for five minutes. The steady states of the first and third phases allow us to correct the baseline of the experimental curves used in the calculation, namely the calorimetric signal and power dissipated in the thermostat. Fig. 3 presents photographs of the position of the sensor in each phase.

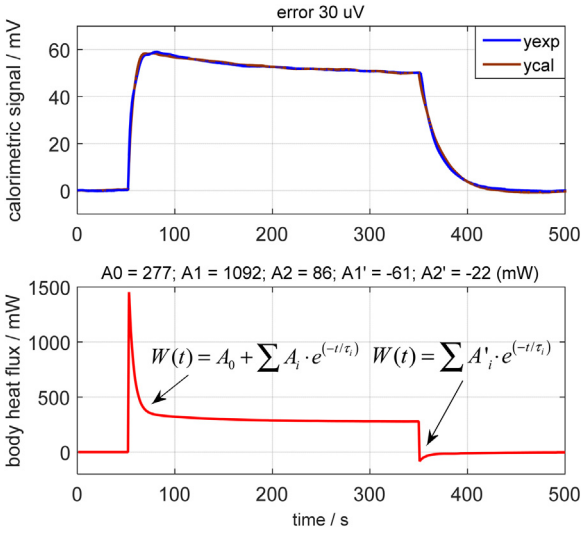

Fig. 5. Body heat flux that passes across the sensor corresponding to the experimental measurement in Fig. 4. For the experimental and calculated calorimetric signals, the error is defined by Eq. (2). The power that passes across the sensor is given by Eq. (3), whose coefficients are A_i and A'_i.

Fig. 4a presents the experimental curves for a standard measurement from the moment of setting the thermostat temperature to the end of measurement, with a total duration of 15 min (900 s). This measurement was performed on the left hand of a 24-year-old male subject in a resting state. The thermostat was set to 24 °C and the room temperature was 23.2 °C. Fig. 4b presents the three experimental curves with corrected baselines. These curves represent the calorimetric signal, thermostat temperature, and power dissipated in the thermostat W_{pid}.

Fig. 5 presents the results of the calculation process for the power W_{body}. The error criterion used was mean-squared error, which is defined as follows:

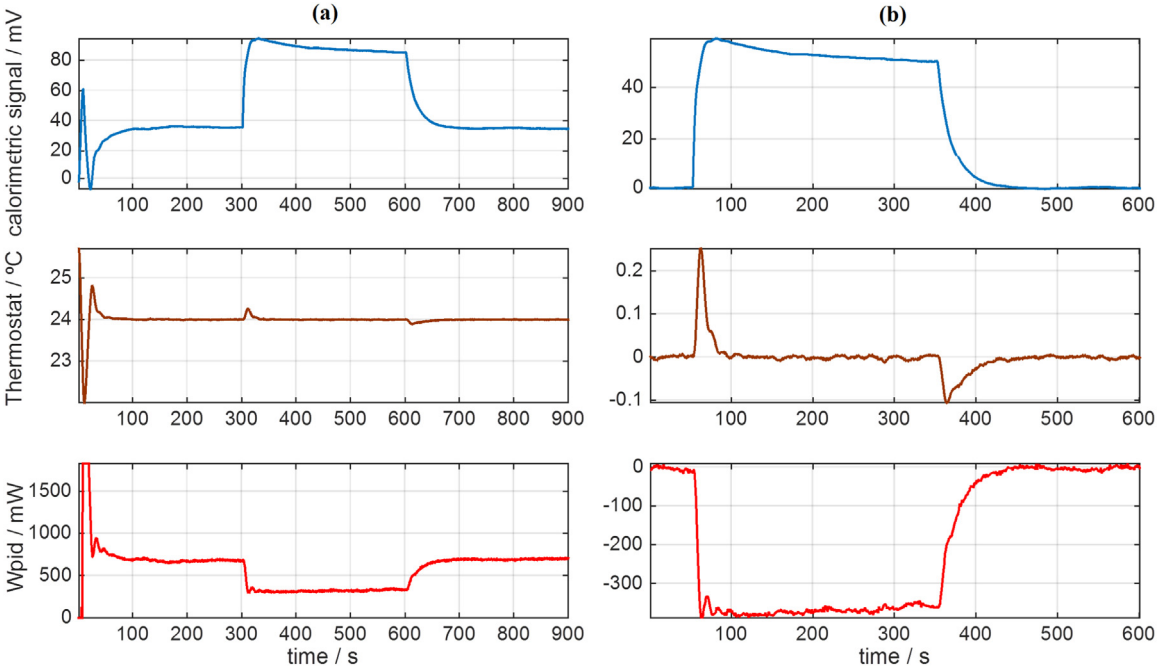

Fig. 4. Experimental curves for measurement on the left hand of a 24-year-old male subject in a resting state with a room temperature of 22.3 °C: a) curves with uncorrected baselines and b) curves with corrected baselines.

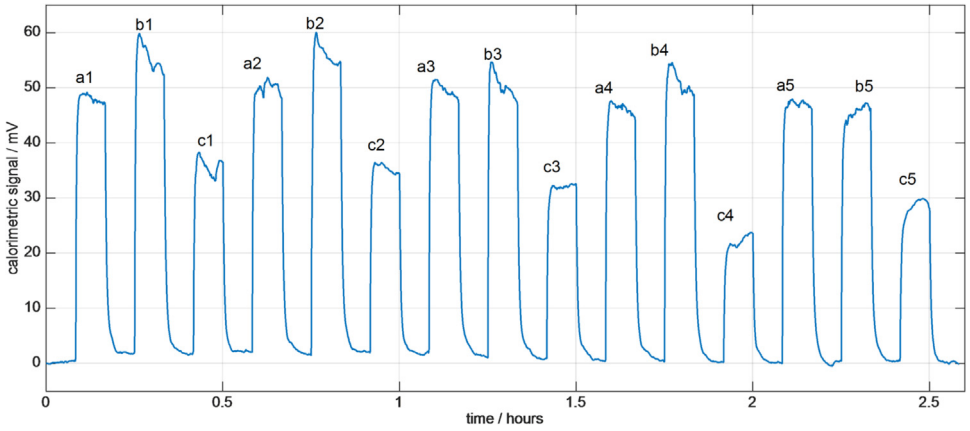

Fig. 6. Calorimetric signal for a series of consecutive measurements on the hand (a1–a5), sternum (b1–b5), and abdomen (c1–c5) for a thermostat temperature of 28 °C (T_{room} = 23 °C). These measurements were performed on a healthy 24-year-old male subject in a resting state (subject 1).

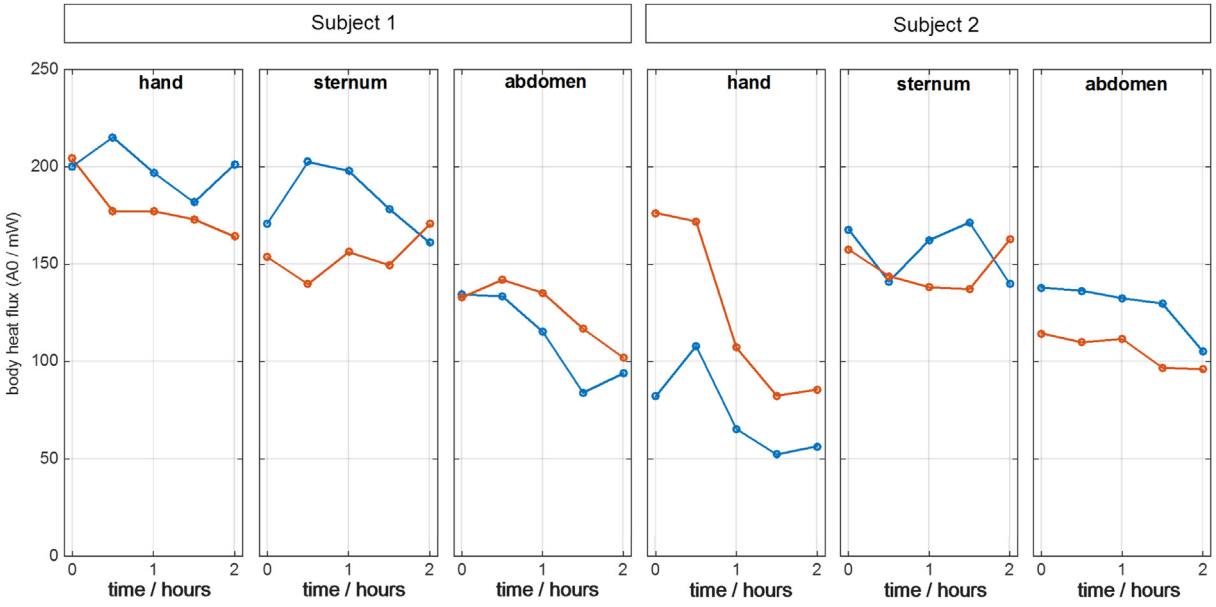

Fig. 7. Temporal variation in the power dissipated (value A_0 in Eq. (3)) from three surface zones of the human body for a thermostat temperature of 28 °C. Measurements were performed on two healthy male subjects with ages of 24 years (subject 1) and 60 years (subject 2).

$$\varepsilon = \frac{1}{N}\sqrt{\sum_{i=1}^{N}(y_{\exp}(i) - y_{cal}(i))^2}\,, \tag{2}$$

where N is the number of points, $y_{exp}(i)$ are the values of the experimental calorimetric signal, and $y_{cal}(i)$ are the values of the calculated signal. The mean-squared error in the reconstruction of the calorimetric signal is $\varepsilon \approx 30\,\mu V$. The power that travels across the sensor is calculated as follows:

$$\begin{aligned} W(t) &= 0 && \text{for } t < t_1 \\ W(t) &= A_0 + A_1\exp(-t/\tau_1) + A_2\exp(-t/\tau_2) && \text{for } t_1 < t < t_2, \\ W(t) &= A_1'\exp(-t/\tau_1) + A_2'\exp(-t/\tau_2) && \text{for } t > t_2 \end{aligned} \tag{3}$$

where t_1 is the moment the sensor is placed on the human body and t_2 is the instant it is returned to its base. For all performed measurements, we analysed the most appropriate time constants for calorimetric signal reconstruction, which resulted in values of $\tau_1 = 5\,s$ and $\tau_2 = 70\,s$ for both the time interval during which the sensor is placed on the human body and the time interval during which it is returned to its base. The coefficient A_0 is the steady-state power. The coefficient A_1 corresponds to the amplitude of the first exponential associated with a time constant of 5 s and characterises the initial power overshoot, which is a consequence of the temperature difference between the sensor and the human body surface. The coefficient A_2 is the amplitude of the second exponential associated with a time constant of 70 s and characterises the progressive thermal equalisation to reach a steady state. The coefficients A'_1 and A'_2 have the same meanings as A_1 and A_2, respectively, but correspond to the moment the sensor is placed back on the base.

4. Experimental results

We performed measurements on two healthy male subjects with different ages: 24 years (subject 1) and 60 years (subject 2). Both subjects were in a resting state (seated) before and during the measurements and were dressed normally. Neither subject had been exercising prior to the measurements. The room temperature was in the range of 22–24 °C. Measurements were taken from three areas of interest (Maniar et al., 2015): the hand and two parts of the trunk (sternum and abdomen). In the previous section, a typical measurement was described (Fig. 4). However, in practice, we performed a series of consecutive measurements. The sensor was returned to its calibration base between these measurements. This provided initial and final steady states, which made it possible to correct the baselines and calculate the heat power accurately. Before each series of thermal

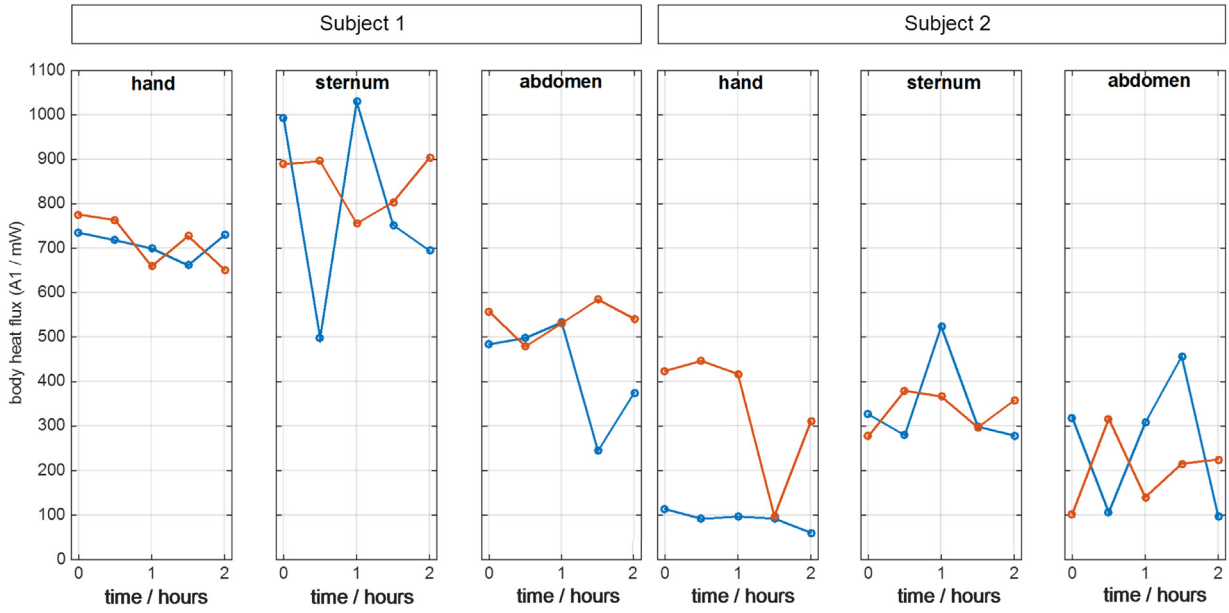

Fig. 8. Temporal variation in the value of A_1 (Eq. (3)) for three surface zones of the human body for a thermostat temperature of 28 °C. Measurements were performed on two healthy male subjects with ages of 24 years (subject 1) and 60 years (subject 2).

Table 2
Mean values of the amplitudes A_i of the power equation (Eq. (3)) for each subject and each area with a thermostat temperature of 28 °C.

	Subject 1			Subject 2			
	Hand	Sternum	Abdomen	Hand	Sternum	Abdomen	Units
A_0	189	168	119	99	152	117	mW
A_1	712	822	483	215	338	229	mW
A_2	32	56	12	24	78	3	mW
A'_1	− 245	− 292	− 212	− 206	− 234	− 208	mW
A'_2	0	14	2	− 14	− 21	− 12	mW

measurements, blood pressure and heart rate were measured for each subject. Normal values were obtained in all cases.

4.1. Temporal study

In this section, we aim to analyse the temporal variation in the heat flux in a defined skin area of the human body for a constant thermostat temperature of 28 °C. Five consecutive measurements were performed in each area of interest, starting with the hand, then the sternum, followed by the abdomen. Fig. 6 presents the calorimetric signal for each of the measurements. The pulses correspond to the heat dissipations in each area (hand, sternum, and abdomen). We performed two series of measurements for each subject.

The heat powers can be determined using the procedure described in the previous section. Fig. 7 presents the values of the steady-state

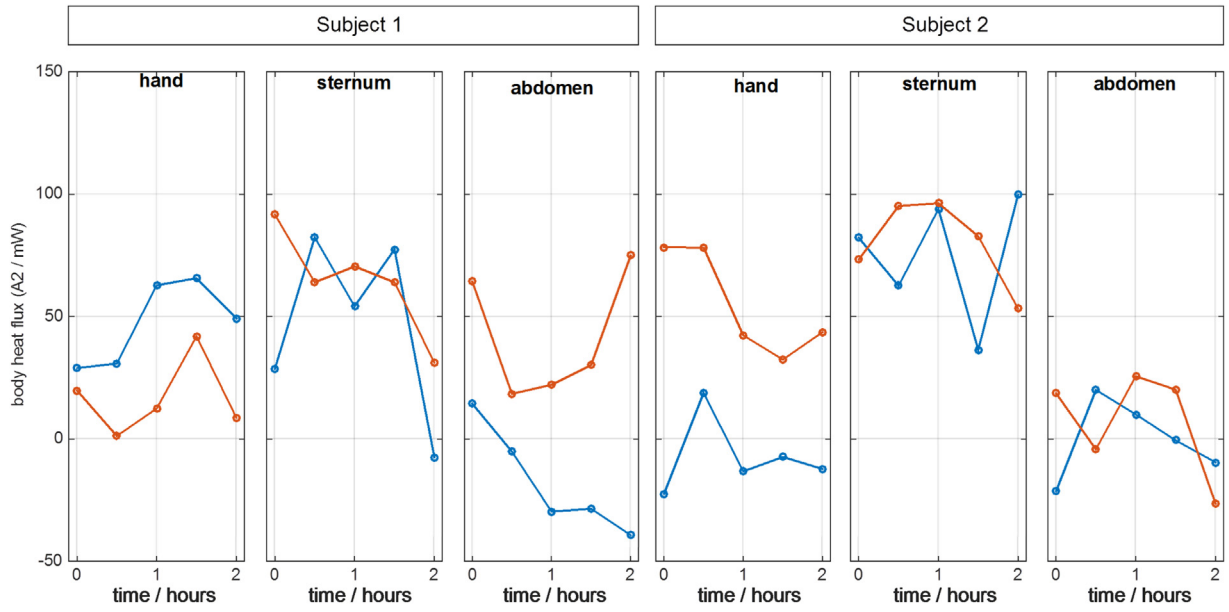

Fig. 9. Temporal variation in the value of A_2 (Eq. (3)) for three surface zones of the human body for a thermostat temperature of 28 °C. Measurements were performed on two healthy male subjects with ages of 24 years (subject 1) and 60 years (subject 2).

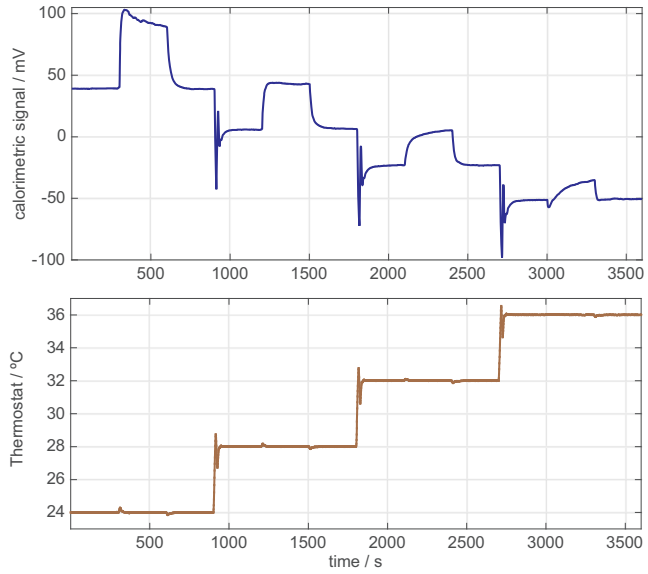

Fig. 10. Calorimetric signal and thermostat temperature for measurements performed on the sternum of subject 1 (24 years old).

dissipated power (parameter A_0 in Eq. (3)) for each subject and each measurement area of the body. For a time interval of 2 h, the power dissipated in the three areas shows a temporal variation of ± 15 to ± 25 mW for subject 1. However, for subject 2, the variation is lesser in the trunk (± 9 to ± 16 mW), but greater in the hand (± 45 mW). In general, the dissipations are greater in subject 1 than in subject 2. The mean dissipation values for subject 1 are 189 mW on the hand, 168 mW on the sternum, and 119 mW on the abdomen. For subject 2, the mean dissipation values are 99 mW on the hand, 152 mW on the sternum, and 117 mW on the abdomen. These dissipations correspond to a measurement area of 4 cm^2 with a thermostat temperature of 28 °C, where T_{room} = 23 °C.

The second term of the power expression (Eq. (3)) corresponds to a "Dirac," which is a consequence of the instant contact between two surfaces with different temperatures, namely the sensor and human body. This exponential has an amplitude of A_1, whose temporal variation is shown in Fig. 8. Table 2 lists the mean values of all amplitudes in Eq. (3). Unsurprisingly, in all cases, the value of A_1 is higher for subject 1 than for subject 2. This is because the surface temperature of subject 1 is higher.

The third term of the power expression (Eq. (3)) represents an exponential with an amplitude of A_2. This term describes the thermal equalisation of the sensor and human body after contact. The time constant for this exponential is 70 s. The values of A_2 for the studied cases are presented in Fig. 9.

In conclusion, we can say that the dissipation (A_0) in the sternum is higher than that in the abdomen for both subjects. Additionally, the values of amplitudes A_1 and A_2 are higher in the dissipations measured on the sternum than in those measured on the hand or abdomen. Generally, all amplitudes are higher for subject 1 than for subject 2, except for A_2, which is slightly higher for the older subject (subject 2) for the dissipation measured on the sternum.

Furthermore, amplitudes A'_1 and A'_2 in Eq. (3) are related to the transient state prior to reaching thermal equilibrium between the sensor and calibration base. From Table 2, we can deduce that the absolute value of A'_1 is higher for subject 1 than for subject 2 based on the higher temperature of subject 1. Additionally, the value of A'_1 for the sternum is higher than that for the other areas for both subjects. The same is true for A_0 and A_1.

4.2. Study of heat dissipation as a function of the temperature of the thermostat

Predictably, when we increase the thermostat temperature, the measured heat power decreases. Experimentally, we can prove the linear relationship between the thermostat temperature $T_{Thermostat}$ and measured power $W_{body} = \dot{q}$. The slope of the line represents the thermal conductance C between the thermostat and a point inside the body with a temperature of T_{core}, where $C = \dot{q}/(T_{Thermostat} - T_{core})$. Based on this thermal conductance value, it is possible to determine the total thermal resistance (R_T = 1/C in K/W) between the skin of the human body and the thermostat. Having experimentally determined the sensor's thermal resistance R_{sensor} to be 12 K/W (Socorro et al., 2017), we can estimate the human body resistance based on the hypothesis of having two resistors in series. In this case, the resistance of the human body would be $R_{body} = R_T - R_{sensor}$.

To study this thermal resistance, we performed measurements on both subjects using the same areas of the human body surface as before,

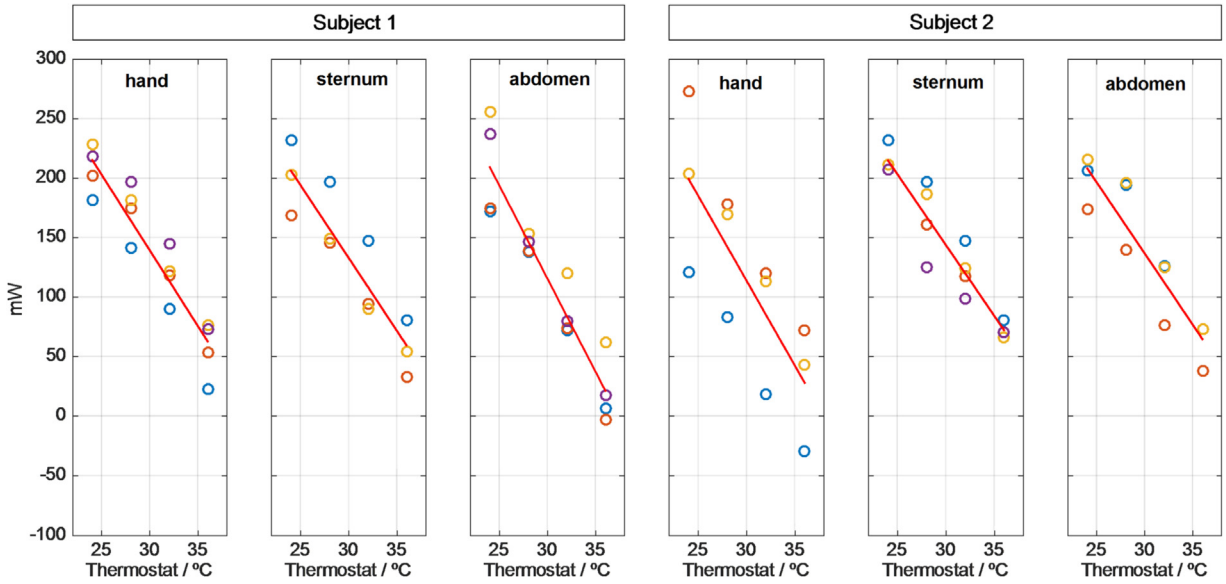

Fig. 11. Power dissipated by the human body A_0 as a function of thermostat temperature for different surface areas on the human body for two healthy male subjects with ages of 24 years (subject 1) and 60 years (subject 2). Circles of the same colour correspond to the same series of consecutive measurements as shown in Fig. 10.

Table 3
Thermal resistance in K/W.

Zone	Subject 1	Subject 2
Hand	65 ± 3	57 ± 8
Sternum	68 ± 4	71 ± 6
Abdomen	50 ± 8	70 ± 6

namely the hand, sternum, and abdomen. Each series of measurements consisted of four measurements that were performed sequentially for four thermostat temperatures: 24, 28, 32, and 36 °C. Fig. 10 presents the calorimetric signal and thermostat temperature for measurements performed on the sternum of subject 1.

Fig. 11 presents the power dissipated by the human body A_0 for each subject and each measurement area as a function of thermostat temperature. The red lines represent the results of linear regression. The resistance of the human body is equal to the inverse of the slope of the line minus the sensor's thermal resistance. Table 3 lists the resistance results. To determine the variation in resistance, we calculated the slope of each line corresponding to each series of measurements and compared it to the average slope obtained for all measurements performed on that zone and subject. The results show that this variation is less than 12.8%. These experimental results can be considered as reference values for future investigations. However, the dispersion of the numerical results suggests that a broader study with more subjects is required to establish an accurate range of values. Furthermore, these values may be altered by different physiological or pathological conditions, which could be the subject of further research.

5. Conclusions

The presented calorimetric sensor is a useful tool for the physiological study of the human body and can serve as a valuable complement to studies based on thermographic technics. In this paper, we presented measurements performed with the sensor that reveal the levels of heat power dissipated when placing the sensor on three different areas of the human body. Sensor placement represents a controlled disturbance on the human body surface that generates a thermal response. The experimental measurements seem to indicate that temporal variability in the heat flux is related to body mechanisms for maintaining a stable core temperature. Furthermore, the sensor allowed us to identify a specific parameter for the body that we defined as thermal resistance, which is different for each measurement area on the body. The heat power and thermal resistance values presented in this paper may provide a useful starting point for future research. Additionally, the calorimetric sensor presented in this work could serve as a foundation for the construction of a portable device that facilitates continuous measurements over long time periods during any activity.

References

Denoble, A.E., Hall, N., Pieper, C.F., Kraus, V.B., 2010. Patellar skin surface temperature by thermography reflects knee osteoarthritis severity. Clin. Med. Insights Arthritis Musculosketet. Disord. 3, 69–75.

Godoy, S.E., Hayat, M.M., Ramirez, D.A., Myers, S.A., Padilla, R.S., Krishna, S., 2017. Detection theory for accurate and non-invasive skin cancer diagnosis using dynamic thermal imaging. Biomed. Opt. Express 8 (4), 2301–2323.

Haidar, S.G., Charity, R.M., Bassi, R.S., Nicolai, P., Singh, B.K., 2006. Knee skin temperature following uncomplicated total knee replacement. Knee 13, 422–426.

Brown, M.E. (Ed.), 1998. Handbook of Thermal Analysis and Calorimetry: Principles and Practice. Elsevier Science, Amsterdam, The Netherlands.

Hansen, L.D., 2001. Toward a standard nomenclature for calorimetry. Thermochim. Acta 371, 19–22.

Jesús, C., Socorro, F., de Rivera, M.R., 2013a. Development of a calorimetric sensor for medical application. Part II. Identification and Simulation. J. Therm. Anal. Calorim. 113, 1003–1007.

Jesus, C., Socorro, F., Rodríguez de Rivera, M., 2013b. Development of a calorimetric sensor for medical application. Part III. Operating methods and applications. J. Therm. Anal. Calorim. 113, 1009–1013.

Lahiri, B.B., Bagavathiaappan, S., Jayakumar, T., Philip, J., 2012. Medical applications of infrared thermography: a review. Infrared Phys. Technol. 55, 221–235.

Livingston, S., Nolan, R., Frim, J., Reed, L., Limmer, R., 1987. A thermographic study of the effect of body composition and ambient temperature on the accuracy of mean skin temperature calculations. Eur. J. Appl. Physiol. Occup. Physiol. 56, 120–125.

Maniar, N., Bach, A.J.E., Stewart, I.B., Costello, J.T., 2015. The effect of using different regions of interest on local and mean skin temperature. J. Therm. Biol. 49–50, 33–38.

Mehra, A., Langkamer, V.G., Day, A., Harris, S., Spencer, R.F., 2005. Creative protein and skin temperature post total knee replacement. Knee 12, 297–300.

Miyakoshi, N., Itoi, E., Sato, K., Suzuki, K., Matsuura, H., 1998. Skin temperature of the shoulder: circadian rhythms in normal and pathologic shoulders. J. Shoulder Elb. Surg. 7, 625–628.

Nelder, J.A., Mead, C., 1965. A simplex method for function minimization. Comput. J. 7, 308–313.

Ogata, K., 2010. Modern Control Engineering. Prentice Hall, Upper Saddle River, NJ, USA.

Optimization ToolboxTM User's Guide, 2004. 5th Printing; Revised for Version 3.0 (Release 14). The MathWorks, Inc., Natic, MA, USA.

Rajapakse, C., Grennan, D.M., Jones, C., Wilkinson, L., Jayson, M., 1981. Thermography in the assessment of peripheral joint inflammation – a re-evaluation. Rheumatol. Rehabil. 1981 (20), 81–87.

Rokita, E., Rok, T., Taton, G., 2011. Application of thermography for the assessment of allergen-induced skin reactions. Med. Phys. 38, 765–772.

Socorro, F., Rodríguez de Rivera, P.J., Rodríguez de Rivera, Mi, Rodríguez de Rivera, M., 2017. Mathematical model for localised and surface heat flux of the human body obtained from measurements performed with a calorimetry minisensor. Sensors 17, 2749.

Socorro, F., de Rivera, M.R., 2010. Development of a calorimetric sensor for medical application. Part I. Operating model. J. Therm. Anal. Calorim. 99, 799–802.

Socorro, F., Rodriguez de Rivera, P.J., Rodríguez de Rivera, M., 2016. Calorimetric minisensor for the localized measurement of surface heat dissipated from the human body. Sensors 16, 1864.

Vecchio, P.C., Adebajo, A.O., Chard, M.D., Thomas, P.P., Hazleman, B.L., 1992. Thermography of frozen sholder and rotator cuff tendinitis. Clin. Rheumatol. 11, 382–384.

Wendlandt, W.W., 1974. Thermal Methods of Analysis. John Wiley and Sons, New York, NY, USA.